ELSEVIER

Marine and Petroleum Geology 22 (2005) 569–578

Marine and Petroleum Geology

www.elsevier.com/locate/marpetgeo

The spatial scales, distribution, and intensity of natural marine hydrocarbon seeps near Coal Oil Point, California

Libe Washburn[a,c,*], Jordan F. Clark[b], Phaedon Kyriakidis[c]

[a]*Department of Geography, Institute for Computational Earth System Science, Santa Barbara, CA 93106, USA*
[b]*Department of Geological Sciences, University of California, Santa Barbara, CA 93106, USA*
[c]*Department of Geography, University of California, Santa Barbara, CA 93106, USA*

Received 16 November 2003; accepted 31 August 2004

Abstract

Natural hydrocarbon seepage from marine environments is an important source of methane and other gases to the atmosphere. Quantifying this flux is necessary for constraining global budgets and understanding local air pollution sources. A field of strong hydrocarbon seepage offshore of Coal Oil Point near Santa Barbara, California produces extensive areas of bursting bubbles at the sea surface. An instrumented buoy was deployed in the Coal Oil Point field to measure directly the atmospheric gas flux from three seeps of varying size and intensity. Spatial scales of continuity of the seeps, quantified by semivariograms, are small, ranging from <1 to about 9 m such that flux values on larger scales are uncorrelated. These de-correlation scales are comparable to the horizontal extents of individual bubble plumes estimated visually at the sea surface. Semivariograms for each seep are used in an ordinary Kriging procedure to interpolate flux measurements onto a regular grid and produce objective maps of the spatial distribution of flux. Spatial integrals yield total flux estimates from the three seeps of $\sim$7400 m^3 day^{-1} which amount to 4–13% of the total flux from the Coal Oil Point field based on estimates from previous studies.

Keywords: Seeps; Seeps oil; Hydrocarbon indicators; Marine environment; Methane

1. Introduction

Natural hydrocarbon seepage from marine environments is an important source of atmospheric methane, an important greenhouse gas. Seeps have been located along most continental margins and are often associated with relatively shallow gas hydrate accumulations and deeper hydrocarbon deposits (e.g.Wilson et al., 1974; Kvenvolden, 1993; Buffet, 2000). The spatial distribution and scales of seep intensity (gas flux per unit area) are not well established, either globally or within strong source areas such as near Coal Oil Point. Furthermore, emission rates from individual vents typically vary over short time scales (minutes to hours, e.g. Tyron et al., 1999; Boles et al., 2001) indicating the need for long term monitoring to establish mean seepage rates. Nevertheless, global estimates have been made using the few existing measurements and an assumed distribution of seep size (e.g. Hovland et al., 1993; Hornafius et al., 1999; Judd et al., 2002).

In this study we examine gas flux distributions at the sea surface from three individual seepage areas within the larger Coal Oil Point (COP) seep field which is located along the northern margin of the Santa Barbara Channel near Santa Barbara, CA. This field is one of the world's strongest hydrocarbon seep regions (Hornafius et al., 1999) and probably contains some of the largest individual marine seeps in the world. Previous observations at the COP field (e.g. Quigley, 1997; Egland, 2000) have shown that bubbling gas flux at the sea surface results from two components: small areas of very intense bubble plumes, and much broader areas of diffuse seepage composed of much smaller bubble plumes. The relative contributions from these components must be determined to quantify the total gas flux to the atmosphere from seep fields such as COP. We focus on small areas of intense seepage which we hypothesize dominate the total flux of methane to the atmosphere from the COP field. This hypothesis is

* Corresponding author. Address: Department of Geography, Institute for Computational Earth System Science, Santa Barbara, CA 93106, USA. Tel.: +1 805 893 7367; fax: +1 805 89 2578.
E-mail address: washburn@icess.ucsb.edu (L. Washburn).

0264-8172/$ - see front matter © 2005 Elsevier Ltd. All rights reserved.
doi:10.1016/j.marpetgeo.2004.08.006

supported by recent observations of Leifer et al. (2000) and Clark et al. (2003) which indicate that large plumes (areas of stronger flux) modify the local marine environment, creating distinct columns of rising seawater and bubbles within the ambient ocean. Here, ambient ocean is the unmodified water column found away from the bubble plumes. Most significantly, these authors showed: (1) the upwelling velocity of the rising plume water is large, 0.2 to >1 m/s; (2) the concentration of methane in the rising plume water is more than four orders of magnitude greater than ambient ocean concentrations; and (3) the plume water can become saturated with respect to the bubbles' methane concentration. Therefore, the fraction of methane released at the seafloor that is emitted to the atmosphere is much larger than would occur if the bubbles were rising through the (methane-unsaturated) ambient ocean.

To determine the contribution due to small areas of strong seepage, observations were made at three seeps using a specialized instrument, called a flux buoy, which measures bubbling flux at the sea surface using a gas capture technique (for a description of the instrument, see below and Washburn et al. (2001)). The seeps were selected to represent three distinct patterns of seepage characterizing the large, intense seeps found in the COP field. The principal research objectives were to: (1) estimate objectively the spatial scales of strong flux, (2) determine the spatial distribution of bubbling gas flux at the sea surface within individual areas of strong seepage, and (3) quantify the total flux of gas coming from these areas. Fluxes could then be compared with previous estimates of the total flux from the COP seep field. These are the first direct, high resolution flux observations of hydrocarbon seepage at COP, and possibly the first from any marine seep field.

2. Field site

Observations of bubbling gas flux were made at three seeps in the COP seep field (rectangles, Fig. 1). All of these seeps are characterized by large sea surface expressions of bursting bubbles and by very strong sonar returns observed during numerous sonar mappings of the field (Quigley, 1997; Hornafius et al., 1999; Quigley et al., 1999). One seep, referred to as 'La Goleta Seep', is located over the South Ellwood anticline in water depths around 65 m. The other two, 'Horseshoe Seep' and 'Shane Seep' are located inshore over the COP anticlines in depths of about 40 and 20 m, respectively. Direct observations of the seafloor have been made only at Shane Seep. These in situ observations have shown that the bubbles emanate from numerous vents (on the order of 10^3), although they are concentrated at three mud and tar volcanoes. The vents are distributed over a seafloor area similar in size to the area of bursting bubbles at the sea surface. Presumably, La Goleta and Horseshoe Seeps have similar seafloor morphologies with bubbles emanating from numerous distinct seafloor vents. Table 1 summarizes nominal locations and area estimates for the three seeps. Additional details on the geological setting of the COP seep field are given by Quigley (1997), Hornafius et al. (1999) and Quigley et al. (1999).

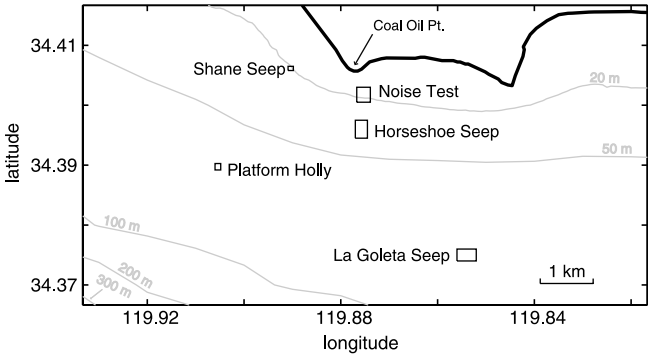

Fig. 1. Map of Coal Oil Point study area showing locations of Horseshoe, La Goleta, and Shane Seeps. The location of a test to determine noise levels of the measurement technique is labeled noise test. Rectangles indicate areas shown in Fig. 2. Platform Holly is an oil production platform. Gray lines are bathymetric contours.

Visual observations made during shipboard sampling suggested that Shane and Horseshoe Seeps were the most intense and that La Goleta was the weakest of the three. A fourth site on the 20 m isobath, containing no visible bubbles, was sampled to establish the noise characteristics of the measurement technique. Hereafter, this site is referred to as 'noise test' (Fig. 1). All measurements at this location resulted from the combined effects of ocean surface gravity waves and buoy motions with no contribution from actual seepage.

3. Methods

3.1. Flux measurement

Gas flux $\dot{q}$ was quantified using an instrument called a flux buoy which floats on the sea surface and measures flux by capturing rising gas bubbles A cone forming the base of the instrument directs rising bubbles into a collection chamber where the differential pressure, Δp, between the gas in the chamber and seawater outside, is measured every second. A computer in a pressure case on the instrument records Δp and releases gas in the chamber at a pre-determined threshold of Δp. This prevents underestimation of flux due to gas overflowing the collection chamber. Absolute pressure and temperature are measured at the top of the collection chamber, 2.6 m below the sea surface, so that gas collected at the chamber depth can be corrected to standard conditions (20 °C, 1 atm) using the ideal gas law. The cone, collection chamber, and pressure case containing the computer and instrument electronics are mounted at the bottom of a hollow spar buoy, 0.09 m in diameter and 3.1 m long. A collar of closed-cell foam around the spar buoy provides additional floatation. The spar buoy configuration was chosen to reduce

Table 1
Summary of seep parameters and sampling

Seep	Location	Sampling dates	Number samples[a]	Maximum flux (m day^{-1})	L (m)	B (m^2 day^{-2})	Total flux[b] (m^3 day^{-1})	Total flux − lower bound[c] (m^3 day^{-1})	99% noise threshold (m day^{-1})	Area[d] (m^2)
Horseshoe	34° 23.757′, 119° 52.530′	17 January 2003	12,736	10	2.81	1.25	4500	3400	0.48	2340
La Goleta	34° 22.523′, 119° 51.258′	20 June 2003	13,356	8.1	1.98	2.25	1900	800	1.0	480
Shane	34° 24.363′, 119° 53.423′	23 August 2002	13,216	24	0.18	14.4	3300	3200	0.43	1350
Noise test	34° 24.125′, 119° 52.995′	19 September 2002	7191	1.6	4.8	0.13	−24[e]	–	–	–

[a] Because the sampling rate was 1 sample s^{-1}, the number of samples (−1) is also the sampling time in seconds.
[b] Spatial integral for all flux values, including noise.
[c] Spatial integral for flux exceeding 99% noise threshold values.
[d] Area corresponding to the total flux − lower bound.
[e] Note that −24 m day^{-1} is the difference between the spatial integrals of the positive and negative values for the noise test which are 960 and −984 m^3 day^{-1}, respectively.

vertical movements of the instrument due to surface waves. During operation, the horizontal position of the flux buoy is measured to within a few meters every 2 s by a differential GPS receiver mounted on the buoy.

In postprocessing, flux data are converted from digital counts to engineering units as described by Washburn et al. (2001). Calibration coefficients were verified between field sampling episodes by operating the buoy in a swimming pool over a metered bubbling gas source. $\dot{q}$ is expressed in units of m^3 per day of gas flux per m^2 of sea surface area, or just m day^{-1}. To reduce the effects of surface waves, flux time series were smoothed using a 5-pole low pass Butterworth filter (with MATLAB analysis software) with a half power cutoff frequency of 1/45 s^{-1}. GPS position data were smoothed with a similar low pass filter but with a cutoff frequency of 1/25 s^{-1} and then interpolated into the flux time series based on time. The resulting data set has smoothed flux and position time series estimated every second along spaghetti-like trajectories (e.g. Fig. 2) centered over regions of intense bursting bubbles.

3.2. Spatial statistics

The spatial scales of the seeps were determined using standard geo-statistical techniques such as described by Isaaks and Srivastava (1989). Semivariogram $\gamma(h)$ estimates were used to establish objectively the spatial scales of continuity of seepage. $\gamma(h)$ is estimated from observations as

$$\hat{\gamma}(h) = \frac{1}{2N(h)} \sum_{(i,j)|h_{ij}=h} (\dot{q}_i - \dot{q}_j)^2 \quad (1)$$

where $\dot{q}_i$ and $\dot{q}_j$ are flux measurements at positions i and j. Following Isaaks and Srivastava (1989), the notation $(i,j)|h_{ij}$ indicates summation over N pairs of points separated by the spatial lag vector h_{ij} which points from location i to location j with length h. Because they were highly variable, but exhibited no preferential directions of variability on the scales of bubble plumes, flux measurements were paired based only on their spatial lag distances h, not their vector separations h_{ij}. For small h, flux values are more likely to be similar so the differences $q_j - q_i$ are likely small, resulting in small $\hat{\gamma}(h)$. For large h, the flux values are more likely to be unrelated resulting in larger differences $q_i - q_j$ and larger values $\hat{\gamma}(h)$. $\hat{\gamma}(h)$ typically reached a nearly constant level for large h corresponding to the variance of these data. The distance over which $\hat{\gamma}(h)$ transitions to a nearly constant level is taken as the spatial scale of continuity for a particular seep.

For the three seep areas and the noise test, $\hat{\gamma}(h)$ was evaluated for 21 spatial lags h ranging from 0.25 to 70 m. Lag spacing was decreased for small h to resolve small scale spatial variability caused by individual bubble plumes. Since few pairs of points were separated by exactly these h values, points were paired if they fell within a tolerance $h \pm \Delta h$ where $\Delta h = 0.2\,h$. Due to the large number of data points recorded at each of the three seeps (up to ~13,000 points, see Table 1), it was not practical to evaluate $\hat{\gamma}(h)$ for all possible pairs of points. Instead, $\hat{\gamma}(h)$ was estimated from 50 ensembles of 1000 points chosen randomly from each seep. This produced 50 estimates of $\hat{\gamma}(h)$ at each of the 21 values of h.

To estimate objectively the scale of spatial continuity L for each seep, a simple exponential of the form

$$\gamma(h) = B[1 - e^{-h/L}] \quad (2)$$

was fitted to the ensemble of 50 values of $\hat{\gamma}(h)$ for all h. This model describes one of the common forms of semivariograms (Isaaks and Srivastava, 1989): a rapid linear increase

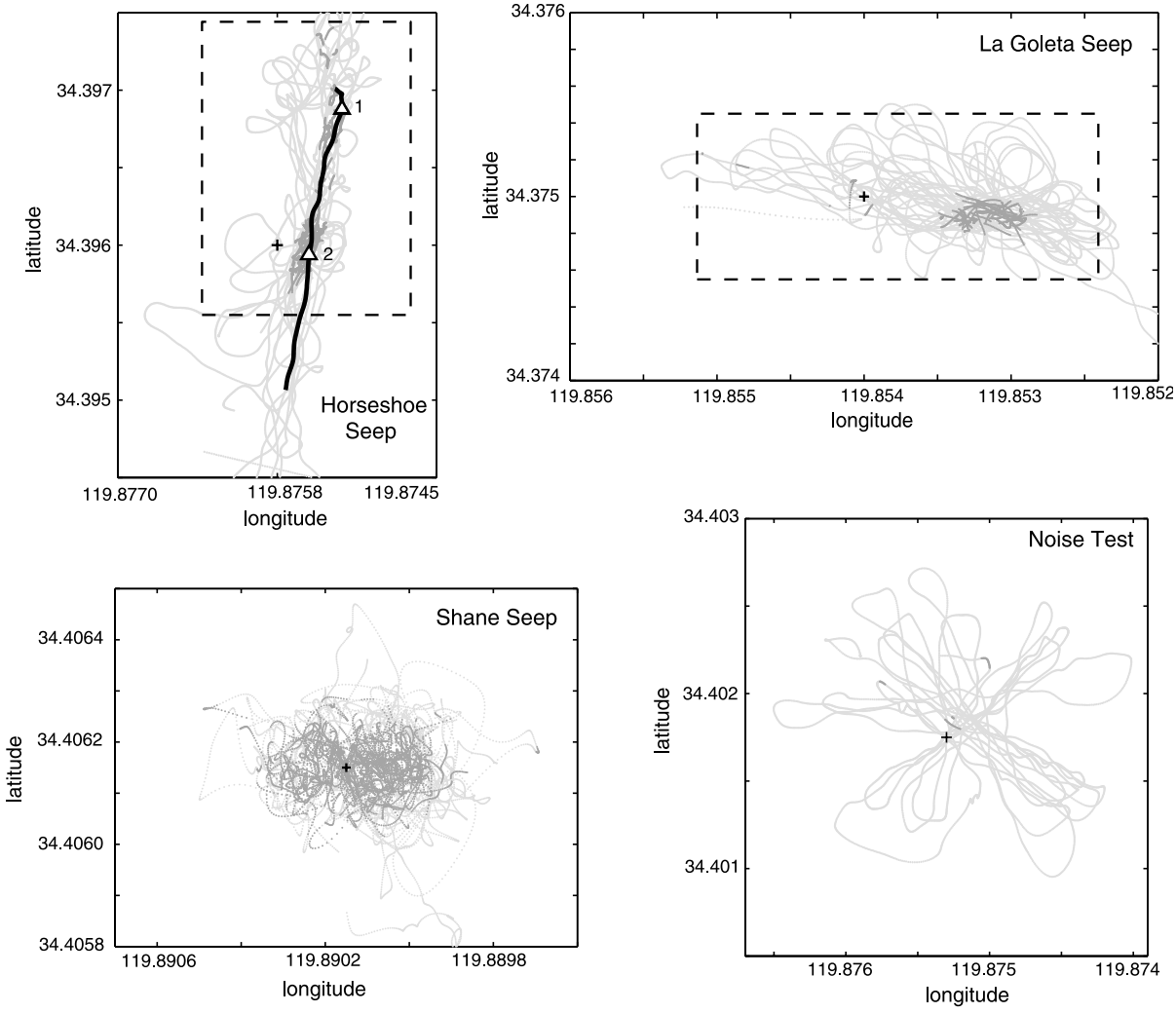

Fig. 2. Light gray lines show paths of flux buoy for: (a) Horseshoe Seep; (b) La Goleta Seep; (c) Shane Seep; and (d) the noise test. Dark gray areas are sections of the buoy tracks where $\dot{q} \geq 1$ m day^{-1}. Profile of Fig. 4 was recorded along path shown by black line in Fig. 2a. Triangles in Fig. 2a indicate maxima along profile of Fig. 3. Dashed rectangles in panels (a) and (b) are the areas contoured in Fig. 6a and b. Plus signs (+) mark the origins of the relative distance coordinates of Fig. 6.

in $\hat{\gamma}(h)$ for small h followed by steadily slower increases for larger h. At very large h the semivariogram reaches a nearly constant value which is approximately proportional to the variance. The parameters B and L are often called the sill and range of the semivariogram, respectively. The sill of the semivariogram is a measure of the square of the expected difference between two observations separated by distances larger than those over which spatial correlation exists (Isaaks and Srivastava, 1989). The range estimates the largest distance over which this spatial correlation exists. At times, a discontinuity exists at the origin in real semivariograms which is the so-called 'nugget effect'. A non-zero nugget effect can indicate unresolved variability at scales smaller than the minimum sampling scale. For each ensemble, B was estimated as the average of $\hat{\gamma}(h)$ for h in the range 10–70 m. Using this value of B, L was then determined by finding the value that minimized the mean squared difference between the observations and model over the ensemble, $[\hat{\gamma}(h) - \gamma(h)]^2$.

Total flux from each seep was estimated by first objectively mapping $\dot{q}$ onto a grid of spatial points using (2) in an ordinary point Kriging procedure (e.g. Isaaks and Srivastava, 1989). Surfer software, version 7.0 was used for Kriging. A separate semivariogram was used for each seep. Prior to the Kriging procedure, closely-spaced data points (<2 m separation) were averaged together to reduce the number of points handled by the Kriging algorithm. Up to 10 averaged data points within a 5 m search radius were combined in the Kriging procedure to produce each grid point estimate. Due to the density of sampling, however, 10 points (and often many more) occurred within a few meters of a typical grid point. After experimentation, a grid spacing of $\Delta x = \Delta y = 2$ m was found to produce spatial flux patterns which compared well with flux patterns measured directly

along the buoy trajectories. Total flux for each seep was estimated by computing the spatial integral of flux values over the grid for the seep.

4. Results

4.1. Spatial scales of continuity of surface gas flux

Sampling at Horseshoe Seep on 17 January 2003 revealed a narrow region of strong flux ($\dot{q} \geq 1$ m day^{-1}, shown by dark gray dots in Fig. 2a), measuring about 20 m east-to-west by 200 m north-to-south. The flux at the northern end of the region was more diffuse. At La Goleta Seep, sampling on 20 June 2003 revealed a single region of strong flux activity (dark gray dots, Fig. 2b), spread over an area of about 60 by 20 m. A few, much smaller areas west of the main activity at La Goleta Seep with $\dot{q} \geq 1$ m day^{-1} may have resulted from small isolated bubble plumes, or from artifacts caused by surface waves or buoy motion. Shane Seep, the most compact of the three seeps, was a roughly elliptically-shaped region about 40 by 25 m (dark gray dots, Fig. 2c).

The histogram of $\dot{q}$ for Horseshoe Seep (Fig. 3a) is similar to those of La Goleta and Shane Seeps (not shown): it is strongly skewed toward positive values with a mode near zero. The maximum flux values at Horseshoe Seep was $\sim$10 m day^{-1} (arrow above x-axis in Fig. 2a). Maximum values at La Goleta and Shane Seeps were 8.1 and 24 m day^{-1}, respectively (Table 1). The mode of the distribution for Horseshoe Seep is centered on 0.05 m day^{-1} (bin width = 0.1 m day^{-1}) and drops off rapidly as $\dot{q}$ increases. In contrast, the histogram for the noise test is nearly symmetric with an approximately Gaussian shape (Fig. 3b).

Negative $\dot{q}$ values in the histograms for Horseshoe Seep and the noise test (and for La Goleta and Shane Seeps histograms, not shown) represent noise resulting from surface gravity waves and buoy motions. As discussed by Washburn et al. (2001), $\dot{q}$ is proportional to the time rate of change of differential pressure, $\mathrm{d}\Delta p/\mathrm{d}t$, where t is time. Normally, $\mathrm{d}\Delta p/\mathrm{d}t$ is positive; as seep gasses accumulate in the chamber, Δp increases and the gas–seawater interface in the chamber moves downward. Negative $\dot{q}$ values indicate decreases in Δp from surface wave effects or upward motions of the buoy due to towing by the research vessel. For Horseshoe Seep most negative $\dot{q}$ values were small, falling in the bin centered on -0.05 m day^{-1}. The largest $\dot{q}$ value was -1.5 m day^{-1}, much smaller in magnitude than the maximum of 10 m day^{-1}. To compare the noise distribution with measured flux values, the negative portion of the histogram for Horseshoe Seep (consisting entirely of noise) is reflected across the y-axis (gray line, Fig. 3a). This is a reasonable representation of the positive portion of the noise distribution since the histogram from the noise test is so symmetric (Fig. 3b). Values of the flux histogram corresponding to noise decrease sharply with increasing positive $\dot{q}$ indicating that noise effects are not significant above $\sim$1 m day^{-1} for Horseshoe Seep on this day of sampling.

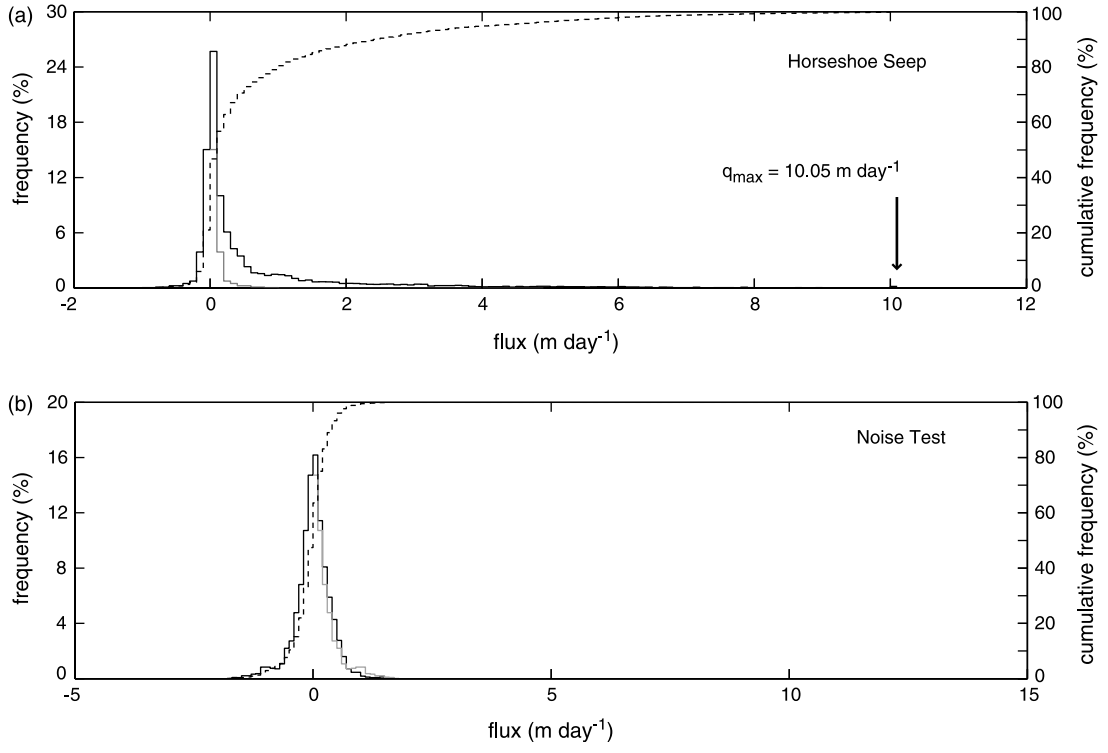

Fig. 3. Histograms of (solid lines) for: (a) Horseshoe Seep and (b) the noise test over the 20 m isobath are indicated on the left hand scale. Cumulative flux (dashed lines) is indicated on the right hand scale. Gray lines show portions of histograms for $\dot{q} < 0$ m day^{-1} reflected across the y-axes.

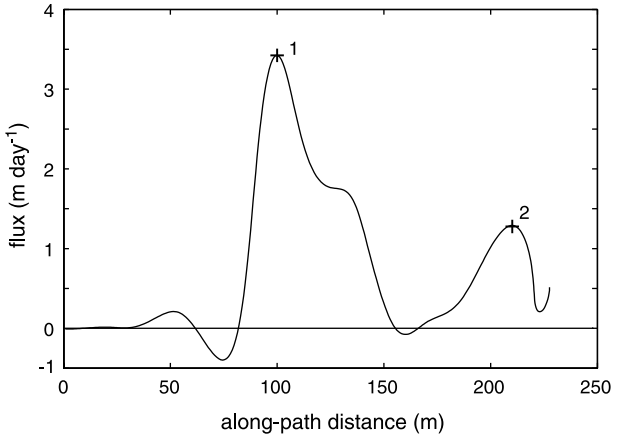

Fig. 4. Profile of $\dot{q}$ at Horseshoe seep along the path shown by black line in Fig. 2a. x-Axis is distance along the path of the flux buoy.

Patterns of flux activity along the sampling paths shown in Fig. 2 suggest that areas of intense seepage extend over horizontal scales of tens of meters. This is confirmed by profiles $\dot{q}$ of along buoy paths as shown by the example in Fig. 4 from Horseshoe Seep. Two sections of the approximately linear buoy path, one $\sim$50 m long and the other $\sim$20 m long, have $\dot{q} \geq 1$ m day^{-1}. Locations of the peaks of Fig. 4, labeled 1 and 2, are indicated by triangles in Fig. 2a. Much smaller scales of spatial continuity are indicated by semivariograms estimates $\hat{\gamma}(h)$. Profiles of the median of $\hat{\gamma}(h)$ ensembles for Horseshoe and La Goleta Seeps generally rise sharply as values of h increase from the smallest lag of $h=0.25$ m (solid lines, Fig. 5), indicating a strong tendency for $\dot{q}$ to be uncorrelated for h larger than a few meters. The drop between the first two median values at La Goleta Seep may result from the high variability at the first lag. Note that log scales are used on both axes because the range in $\hat{\gamma}(h)$ for $h>0$ spans five orders of magnitude and increments of h range from 0.25 to 10 m.

Model fits are consistent with the inference of short scales of spatial continuity indicated by $\hat{\gamma}(h)$: values of L for Horseshoe and La Goleta Seeps are 1.25 and 1.98 m, respectively (Table 1). Shane Seep has even shorter scales with $L=0.18$ m. Profiles of the $\gamma(h)$ using (2) are generally reasonable fits to the median profiles of $\hat{\gamma}(h)$ (dashed lines, Fig. 5). $\gamma(h)$ for Horseshoe and La Goleta Seeps both level out for h greater than $\sim$6 m. In contrast, at Shane Seep $\gamma(h)$ declines sharply for $h>30$ m, possibly the result of under

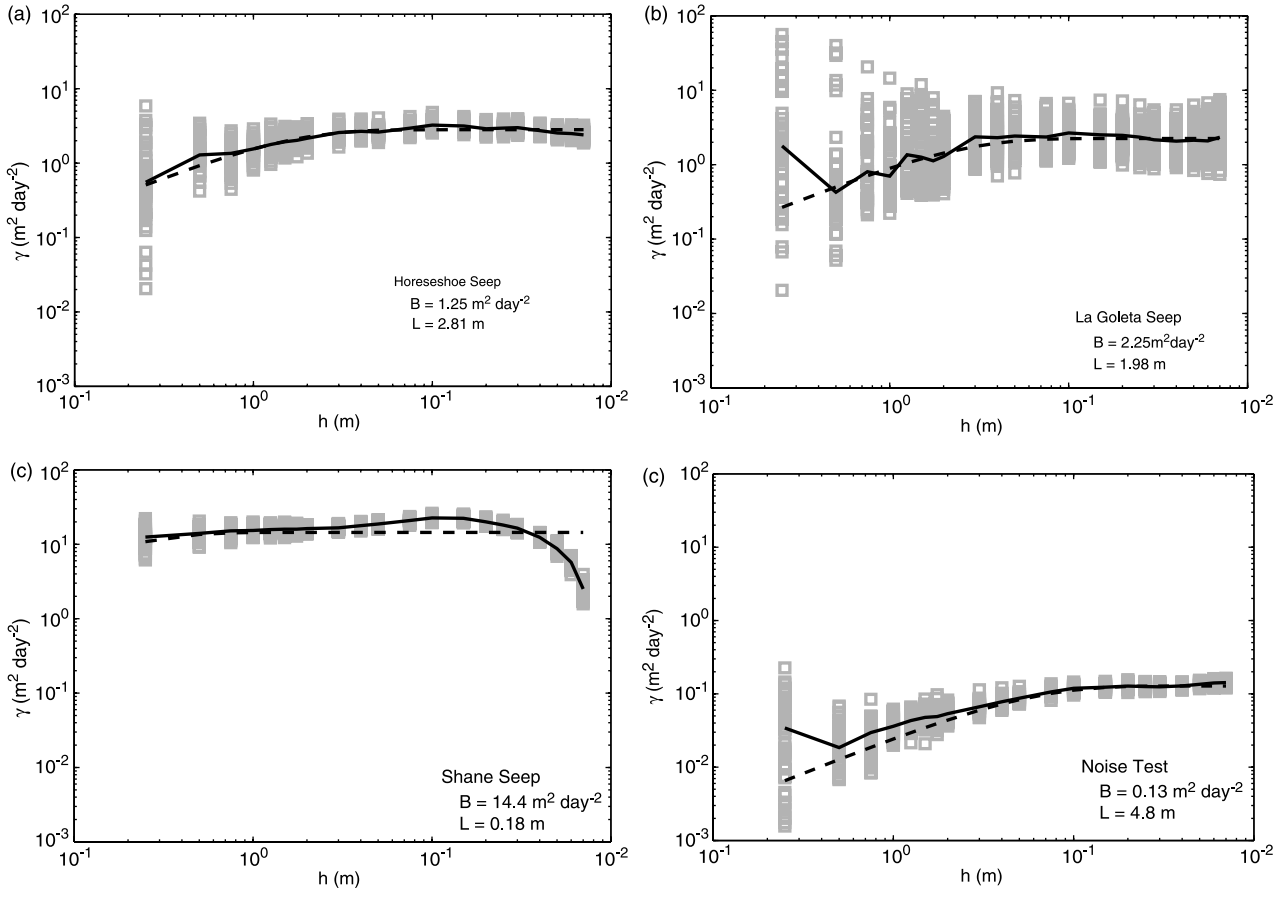

Fig. 5. Ensembles of 50 semivariogram estimates $\hat{\gamma}(h)$ versus spatial lag h (gray squares), for: (a) Horseshoe Seep; (b) La Goleta Seep; (c) Shane Seep; and (d) the noise test. Dotted lines are exponential fits to the ensembles of $\hat{\gamma}(h)$ using Eq. (2). Solid lines connect median values in the ensembles at each lag. Fitted values for L and B from Eq. (2) are shown for each seep.

sampling at these large spatial lags where few estimates of $\gamma(h)$ are available.

Variability in $\hat{\gamma}(h)$ is very large for Horseshoe and La Goleta Seeps as is seen by the extensive spread in the ensembles (gray squares, Fig. 5), particularly for small h. For example, at La Goleta Seep for the first lag of $h=0.25$ m, $\hat{\gamma}(h)$ ranges from 0.02 to 60 m^2 day^{-2}, the upper range of which is much larger than the fitted sill value of $B=2.25$ m^2 day^{-2}. At Shane Seep, on the other hand, $\hat{\gamma}(h)$ scatters around a narrow range compared with Horseshoe and La Goleta Seeps and is more nearly constant for $h<30$ m.

Observations from the noise test indicate that buoy motion and surface waves do not significantly affect $\hat{\gamma}(h)$ over the range of h corresponding to spatial scales of strong flux. An alternating pattern of positive and negative $\dot{q}$ along drift tracks during the noise test was found suggesting a large scale correlation caused by slow oscillations in $d\Delta p/dt$ (periods of 40 s and longer; see Washburn et al. (2001)). The profile of $\gamma(h)$ for the noise test (Fig. 5d) is similar in shape to $\gamma(h)$ profiles for the actual seeps, but with two important differences. First, the range $L=4.8$ m is over twice as large as La Goleta Seep and almost 27 times as large as Shane Seep. Thus, the much larger range for the noise test indicates that buoy motion and surface waves introduce spurious correlation only at scales large compared with the actual scale of strong seepage. Second, the sill value of $B=0.13$ m^2 day^{-2} is at least 10 times smaller than B of the actual seeps. Thus expected differences in $\hat{\gamma}(h)$ due to noise alone are much smaller than those associated with seepage activity.

4.2. Spatial distribution and intensity of surface gas flux

Maps of $\dot{q}$ at each seep and the noise test quantify the spatial distribution of flux at the sea surface Model parameters B and L from (2), summarized in Table 1, were used in the Kriging procedure to interpolate values from the drift trajectories (Fig. 2) onto a regular spatial grid. Maps were constructed from data collected on a single day over a period of a few hours. The sampling time at each seep in seconds equals the number of data samples given in of Table 1. Inclusion of data over relatively short time intervals was necessary because the positions of bubble plumes at the sea surface change due to time-varying ocean currents in the region resulting from tidal, wind, and remote forcing (e.g. Dever et al., 1998; Harms and Winant, 1998; Winant et al., 2003; Dever, 2004). Additionally, the strength of bubble sources on the sea floor also changes on time scales as short as a few minutes to a few hours (Boles et al., 2001; Leifer and Boles, this issue). This variability in seep strength is due to changes in the water column height due to tides and swell and other poorly understood processes.

The spatial maps of $\dot{q}$ shown in Fig. 6 are consistent with the distributions of $\dot{q}\geq 1$ m day^{-1} shown in Fig. 2. At Horseshoe Seep, the gently curving band of high $\dot{q}$ values ($\dot{q}\geq 0.5$ m day^{-1}, light shading) is aligned north-to-south. Flux is stronger in the southern part of the band with $\dot{q}\geq 3$ m day^{-1} (dark shading) over about 20% of the area centered at relative coordinates of -10, 30 m. $\dot{q}$ decreases over the northern part of the band, although another smaller area where $\dot{q}\geq 3$ m day^{-1} is also observed. The origins of the relative coordinate systems used for the spatial maps of Fig. 6 are indicated by plus (+) signs in Fig. 2. The dashed rectangle of Fig. 2a is the area around Horseshoe Seep mapped in Fig. 6a. The estimated total gas flux from the sea surface for Horseshoe Seep over the rectangular area of Fig. 6a is 4500 m^3 day^{-1}, assuming $\dot{q}=0$ m day^{-1} in areas where no measurements were obtained. The total flux estimate includes contributions from seepage plus the effects of noise, although the effects of noise may be small since its distribution is approximately symmetric (Fig. 3b) and therefore largely self-canceling.

To estimate a lower bound on the total flux, a second estimate was computed by integrating the spatial distribution only for positive values $\dot{q}$ exceeding 99% of the noise distribution. The noise distribution at each seep was estimated by reflecting the negative part of the histogram across the y-axis and determining $\dot{q}$ corresponding to the 99th percentile. Table 1 lists the 99% threshold values at each seep; for Horseshoe Seep it is 0.48 m day^{-1} so the lower bound estimate does not include the contribution from areas where $\dot{q}<0.48$ m day^{-1}. The lower bound estimate of total flux for Horseshoe Seep is 3400 m^3 day^{-1} (Table 1). This flux emanates from an area of the sea surface of 2340 m^2 (Table 1).

The spatial map for La Goleta Seep indicates lower values of $\dot{q}$ spread over a smaller area. The total flux over the entire rectangular area of Fig. 6b for La Goleta Seep is 1900 m^3 day^{-1} while the lower bound total flux estimate is 800 m^3 day^{-1} emanating from an area of 480 m^2. The much larger difference in these flux estimates compared with Horseshoe Seep results from the higher 99% threshold flux of 1.0 m day^{-1}, about double the Horseshoe Seep value. Higher surface waves and swell on the day of sampling probably account for the higher 99% noise threshold value at La Goleta Seep.

At Shane Seep, the spatial distribution of flux with $\dot{q}\geq 0.5$ m day^{-1} is an elliptical area; about a third of this area has $\dot{q}\geq 3$ m day^{-1}. The total flux over the area of Fig. 6c is 3300 m^3 day^{-1}. The lower bound total flux estimate is very close to this at 3200 m^3 day^{-1} which emanates from an area of about 1350 m^2.

Values of $\dot{q}$ from the noise test were mapped in the same manner as for the seeps to examine how noise influences total flux estimates. The map of $\dot{q}$ for the noise test shown in Fig. 6d indicates only a few areas where $\dot{q}\geq 0.5$ m day^{-1}, consistent with the histogram of 3b. The total flux for the rectangular area of Fig. 6d is -24 m^3 day^{-1}, much smaller than for the seeps. It is negative because the spatial integral of the negative values (-984 m^3 day^{-1}) slightly exceeds the integral of the positive values (960 m^3 day^{-1}).

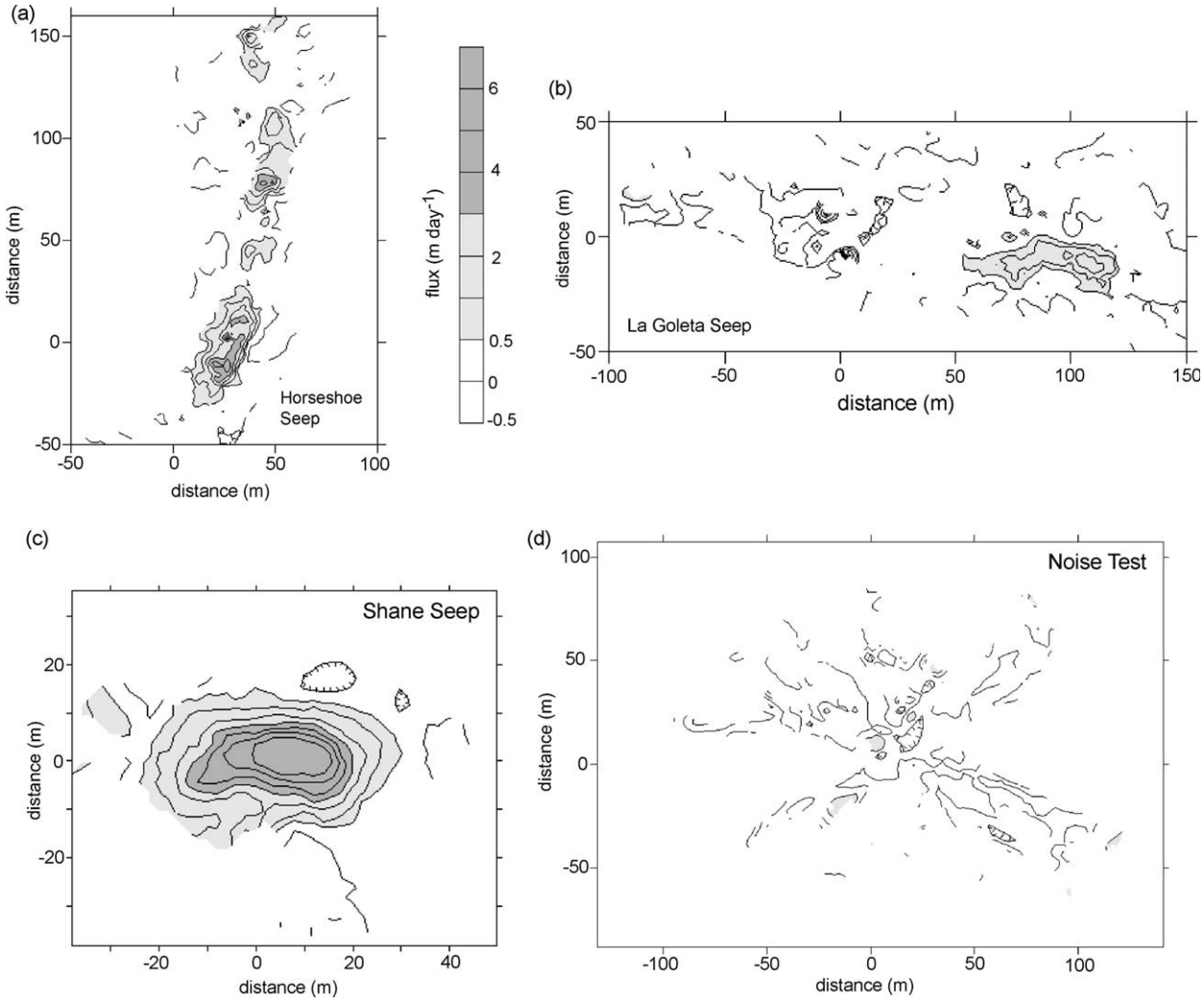

Fig. 6. Contours of $\dot{q}$ for: (a) Horseshoe Seep; (b) La Goleta Seep; (c) Shane Seep; and (d) the noise test. Gray scale indicates $\dot{q}$ in m day^{-1}. x and y-axes give relative distance measured from the origins shown with plus signs (+) in Fig. 2. Areas contoured in panels (a) and (b) are indicated with dashed rectangles in Fig. 2a and b.

5. Discussion and conclusions

Measurements of surface gas flux were $\dot{q}$ made offshore of Coal Oil Point at three natural hydrocarbon seeps, named Horseshoe, La Goleta, and Shane Seeps, during 3 days of sampling in 2002 and 2003. Sampling on a fourth day in 2002 obtained flux measurements in an area away from natural seepage to examine the effects of noise on the measurement technique. Observations were obtained with the flux buoy described by Washburn et al. (2001).

Profiles of $\dot{q}$ (e.g. Fig. 4) indicate that regions of high gas flux extend over scales of tens of meters, consistent with visual observations during sampling of areas of bursting bubbles at the sea surface. This spatial distribution contrasts sharply with the much smaller spatial scales of continuity of $\dot{q}$ estimated objectively from semivariograms $\hat{\gamma}(h)$. We speculate that the difference indicates two fundamental spatial scales of seepage. The larger scale corresponds to groups of individual bubble plumes which are spatially coherent over tens of meters, while the smaller scale results from individual bubble plumes.

The method used to compute $\hat{\gamma}(h)$ may also account for part of the difference because it assumes isotropic distributions of $\dot{q}$. Values of $\hat{\gamma}(h)$ were computed at spatial lags h in the range 0.25–70 m. Exponential fits to $\hat{\gamma}(h)$ in the seeps using (2) yielded estimates for the range L from 0.18 to 2.81 m (Table 1). As discussed by Isaaks and Srivastava (1989), the actual scales of spatial continuity are somewhat larger than L. They suggest a better estimate is the distance over which $\gamma(h)$ attains 95% of its final level which is the sill, B, in (2). This occurs for $h \approx 3L$ so the corresponding spatial scales are from about 0.6 to 9 m. Because $\hat{\gamma}(h)$ was computed based on the magnitude of h but not on its direction, large scale asymmetry in the distributions of $\dot{q}$, such as is evident at Horseshoe and La Goleta Seeps (Fig. 2a and b), tends to increase $\hat{\gamma}(h)$ for large h.

The small scales of continuity estimated from $\hat{\gamma}(h)$ are consistent with the horizontal extent of individual bubble plumes at the sea surface. The shortest scales of continuity were found at Shane Seep. For Horseshoe and La Goleta Seeps, $\hat{\gamma}(h)$ grew rapidly as h increased from small values (although variability was high), suggesting that spatial scales of flux were resolved at these seeps. In contrast, at Shane Seep $\hat{\gamma}(h)$ rose little as h increased from small values; it was nearly constant out to $h \approx 30$ m. This indicates a strong nugget effect at Shane Seep since $\dot{q}$ measurements at the smallest resolved scales are nearly uncorrelated. The diameter of the gas collecting cone on the seep buoy is 0.5 m which is apparently too large to resolve the smallest scales of variability at this seep. This may also account for some of the high variability of $\hat{\gamma}(h)$ at small h at the other seeps. Strong temporal variability in $\dot{q}$ at small scales may also explain the nugget effect at Shane Seep: if large changes in $\dot{q}$ occur over short timescales, then these would be aliased into apparent changes over short spatial scales as the buoy moves over the sea surface.

Total flux estimates for the three seeps were computed along with lower bounds estimated only for $\dot{q}$ exceeding the 99th percentile of the noise distributions (Table 1). For the three seeps combined, the total flux is 7400 $m^3\ day^{-1}$ with a lower bound total of about 4200 $m^3\ day^{-1}$. Quigley (1997) and Hornafius et al. (1999) estimate the total flux for the entire seepage field offshore of COP to be (5.9–19.3)$\times$ 10^4 $m^3\ day^{-1}$ using a sonar technique. Thus, the total flux from the three seeps measured in this study amounts to about 4–12% of the entire field or 2–7% for the lower bound total. Clark et al. (2003) report a preliminary estimate of the flux for Shane Seep of 1900 $m^3\ day^{-1}$ which was based on an average value of $\dot{q}$ and a subjective estimate of seep area. This total is about 40% lower than the range of total flux for Shane Seep given in Table 1. The estimates reported here are likely to be closer to the actual flux because they are based on objectively mapped values of $\dot{q}$.

Time variations in surface gas flux remain to be quantified. Examination of surface flux distributions on different sampling days using the seep buoy suggests that locations of bubble plumes on the sea surface from individual seeps change substantially from day to day. Thus, the locus of all points on the sea surface from which gases are emitted by an individual seep is greater than the instantaneous areas. Consequently, total fluxes obtained by combining data collected over periods of several hours to a few days will likely overestimate true totals. This may explain some of the large range in total flux estimated by Quigley (1997) and Hornafius et al. (1999) since the flux distributions they used were obtained by sonar sampling over multiple days.

Recent observations at Shane Seep described by Clark et al. (2003) show that the bubble gas composition changes rapidly (i.e. on time scales of minutes) during plume rise. They also show that the bubble plumes can produce strong upwelling flows with vertical velocities of $\sim 0.4\ m\ s^{-1}$. Bubble concentrations of methane (CH_4) decrease as dissolved N_2 and O_2 diffuse into rising bubbles from ambient seawater while CH_4 diffuses out. This increases dissolved CH_4 concentrations in ocean waters surrounding the bubble plumes. The higher dissolved CH_4 concentrations then slow CH_4 transfer from the bubbles to surrounding waters. Leifer et al. (2000) demonstrated that, at the largest COP seeps, the water surrounding the bubbles can become supersaturated with respect to bubble CH_4 concentrations and thus CH_4 loss from the bubbles stops. At strong seeps, where bubble rise rates are increased by strong upwelling and dissolved CH_4 concentrations are higher, surface concentrations of CH_4 within the bubbles are likely to be higher compared with weaker seeps. Thus, Clark et al. (2003) hypothesize that stronger seeps are more efficient in transferring CH_4 to the atmosphere.

This hypothesis predicts that regions of strong gas flux such as Horseshoe and Shane Seeps contribute more CH_4 and other hydrocarbons per unit volume of gas emitted than weaker seeps such as La Goleta Seep. Therefore, evaluating the total flux of hydrocarbons to the atmosphere will require simultaneous measurements of bubbling gas flux at individual seeps combined with measurements of gas composition. These studies have already begun at the COP field.

Acknowledgements

We thank Katherine Schwager, David Salazar, and Thor Egland who organized and conducted the field sampling on which this analysis is based. We also thank Gregory Drew and Kyle Visin who assisted in field data collection and calibration of the flux buoy. Gregory Drew also processed the flux buoy data after the field experiments. We thank Eun-hye Yoo who carried out some preliminary spatial analysis of the data. We thank David Farrar and Shane Anderson of the Marine Science Institute at UCSB for their skillful operation of the research vessels during the field experiments. We benefited from helpful conversations with Ira Leifer, Bruce Luyendyk, Jim Bowles, Jean Whelan, Cyril Johnson, and David Menzies during this research. Funding for this research was provided by the University of California Energy Institute.

References

Boles, J.R., Clark, J.F., Leifer, I., Washburn, L., 2001. Temporal variation in natural methane seep rate due to tides, coal oil point area, California. Journal of Geophysical Research (Oceans) 106 (C11), 27077–27087.

Buffet, B.A., 2000. Clathrate hydrates, annual review of earth planetary sciences. Annual Review of Earth Planetary Sciences 28, 477–507.

Clark, J.F., Leifer, I., Washburn, L., Luyendyk, B.P., 2003. Compositional changes in natural gas bubble plumes: observations from the coal oil point marine hydrocarbon seep field. Geo-Marine Letters 23, 187–193.

Dever, E.P., 2004. Objective maps of near-surface flow states near Pt. Conception, California. Journal of Physical Oceanography 34 (2), 444–461, doi: 10.1175/1520-0485.

Dever, E.P., Henderschott, M.C., Winant, C.D., 1998. Statistical aspects of surface drifter observations of circulation in the Santa Barbara channel. Journal of Geophysical Research 103 (C11), 24781–24797.

Egland, E.T., 2000. Direct capture of gaseous emissions from natural marine hydrocarbon seeps offshore of Coal Oil Point, Santa Barbara, California. Masters, Department of Geological Sciences. University of California, Santa Barbara, California, p. 67.

Harms, S., Winant, C.D., 1998. Characteristic patterns of the circulation in the Santa Barbara Channel. Journal of Geophysical Research 103 (C2), 3041–3065.

Hornafius, J.S., Quigley, D.C., Luyendyk, B.P., 1999. The world's most spectacular marine hydrocarbon seeps (Coal Oil Point, Santa Barbara, California): quantification of emissions. Journal of Geophysical Research 104 (C9), 20703–20711.

Hovland, M., Judd, A.G., Burke, J., 1993. The global flux of methane from shallow submarine sediments. Chemosphere 26 (1–4), 559–578.

Isaaks, E.H., Srivastava, R.M., 1989. An Introduction to Applied Geostatistics. Oxford University Press, New York, p. 561.

Judd, A.G., Hovland, M., Dimitrov, L.I., García Gil, S., Jukes, V., 2002. The geological methane budget at continental margins and its influence on climate change. Geofluids 2, 109–126.

Kvenvolden, K.A., 1993. Gas hydrates—geological perspective and global change. Reviews of Geophysics 31, 173–187.

Leifer, I., Boles, J.R., 2005. Measurement of marine hydrocarbon seep flow through fractured rock and unconsolidated sediment. Marine Petroleum Geology, this issue, doi:10.1016/j.marpergeo.2004.10.026.

Leifer, I., Clark, J.F., Chen, R.F., 2000. Modification of the local environment by natural marine hydrocarbon seeps. Geophysical Research Letters 27, 3711–3714.

Quigley, D.C., 1997. Quantifying spatial and temporal variations in the distribution of natural marine hydrocarbon seeps in the Santa Barbara Channel, California. Masters thesis, Department of Geological Sciences. University of California, Santa Barbara, CA, p. 95.

Quigley, D.C., Hornafius, J.S., Luyendyk, B.P., Clark, J.F., Washburn, L., 1999. Decrease in natural marine hydrocarbon seepage near Coal Oil Point, California, associated with offshore oil production. Geology 27 (11), 1047–1050.

Tyron, M.D., Brown, K.M., Torres, M.E., Tréhue, A.M., McManus, J., Collier, R.W., 1999. Measurements of transience and downward fluid flow near episodic methane gas vents, Hydrate Ridge, Cascadia. Geology 27 (12), 1075–1078.

Washburn, L., Johnson, C., Gotschalk, C., Egland, E.T., 2001. A gas capture buoy for measuring bubbling gas flux in oceans and lakes. Journal of Atmospheric and Oceanic Technology 18, 1411–1420.

Wilson, R.D., Monaghan, P.H., Osanik, A., Price, L.C., Rogers, M.A., 1974. Natural marine oil seepage. Science 184 (4139), 857–865.

Winant, C.D., Dever, E.P., Henderschott, M.C., 2003. Characteristic patterns of shelf circulation at the boundary between central and southern California. Journal of Geophysical Research 108 (C2), 3021, doi: 10.1029/2001JC001302.